A molecular dynamics study of N–A–S–H gel with various Si/Al ratios

Chen, Yun; Dolado, Jorge S.; Li, Zhenming; Yin, Suhong; Yu, Qijun; Kostiuchenko, Albina; Ye, Guang

Important note
To cite this publication, please use the final published version (if applicable).
Please check the document version above.

RESEARCH ARTICLE

A molecular dynamics study of N–A–S–H gel with various Si/Al ratios

Yun Chen[1,2] | Jorge S. Dolado[3,4] | Zhenming Li[1] | Suhong Yin[2] | Qijun Yu[2] | Albina Kostiuchenko[1] | Guang Ye[1,5]

[1]Section of Materials and Environment, Faculty of Civil Engineering and Geosciences, Delft University of Technology, Delft, The Netherlands

[2]School of Materials Science and Engineering, South China University of Technology, Guangzhou, Guangdong, China

[3]Centro de Física de Materiales CFM (CSIC-UPV/EHU), Donostia-San Sebastián, Spain

[4]Donostia International Physics Center (DIPC), Donostia-San Sebastián, Spain

[5]Magnel Laboratory for Concrete Research, Department of Structural Engineering, Ghent University, Ghent, Belgium

Correspondence
Jorge S. Dolado, Centro de Física de Materiales CFM (CSIC-UPV/EHU), Donostia-San Sebastián 20018, Spain.
Email: Jorge_dolado002@ehu.eus

Guang Ye, Section of Materials and Environment, Faculty of Civil Engineering and Geosciences, Delft University of Technology, Delft 2628CN, The Netherlands.
Email: G.Ye@tudelft.nl

Funding information
China Scholarship Council, Grant/Award Number: 201906150022; Gobierno Vasco-UPV/EHU, Grant/Award Number: IT1246-19; Spanis Ministry of Science, Innovation and Universities, Grant/Award Numbers: PCI2019-103657, RTI2018-098554-B-I00

Abstract

In this paper, the atomic structures of sodium aluminosilicate hydrate (N–A–S–H) gels with different Si/Al ratios are studied by molecular dynamics simulation. An N–A–S–H gel model was obtained from the polymerization of $Si(OH)_4$ and $Al(OH)_3$ monomers with the use of a reactive force field (ReaxFF). The simulated atomic structural features, such as the bond length, bond angle, and simulated X-ray diffraction pattern of the gel structure are in good accordance with the experimental results in the literature. Si–O–Al is found to be preferred over Si–O–Si in the N–A–S–H gel structure according to the amount of T–O–T bond angles and distribution of $Si^4(mAl)$. Pentacoordinate Al is identified in all simulated N–A–S–H models. It provides strong support to current knowledge that pentacoordinate Al in geopolymer does not only come from raw material. Furthermore, the structural analysis results also show that N–A–S–H gel with lower Si/Al ratios has a more cross-linked and compacted structure.

KEYWORDS
atomic structures, molecular dynamics, N–A–S–H gel, ReaxFF, Si/Al ratio

1 | INTRODUCTION

Sodium aluminosilicate hydrate (N–A–S–H) gel is the primary reaction product of geopolymers.[1,2] The properties of geopolymers are directly related to the nature of N–A–S–H gel. Some basic knowledge of N–A–S–H gel has been obtained through commonly used materials charac-

terization techniques, including X-ray diffraction (XRD) analysis, Fourier transform infrared (FTIR) spectroscopy, and nuclear magnetic resonance (NMR) spectroscopy. All XRD patterns of N–A–S–H gel have a typical hump at 25°–40° 2θ, considered an amorphous or nanocrystalline phase.[3,4] FTIR results have yielded important information about the evolution of N–A–S–H gel during alkali

activation: Al-rich gel is formed in early age and then evolves into an Si-rich gel.[5,6] NMR turns out to be the most contributed technique to reveal the bonding environment within N–A–S–H gel. Traditionally, many researchers believed that most Si and all Al are tetrahedrally linked by bridging oxygens, that is, Q^4. Although traces of Al(V) and Al(VI) can be found in geopolymer pastes, these five/six coordinated Al sites are believed to belong to raw materials, like fly ash or metakaolin.[7,8] However, Walkley et al. also found small amounts of Al(VI) in two geopolymer pastes, but the authors assigned it to reaction product paragonite instead of N–A–S–H gel based on XRD results.[9] More recently, Al(VI) has been detected, for the first time, in synthetic hydrous sodium aluminosilicate gel through multiple quantum magic angle spinning spectroscopy by Walkley.[10] These six coordinated Al sites were described as charge-balancing extra-framework Al species. Despite all of these achievements, due to the complex nature of N–A–S–H gel, these experimental techniques are not able to fully unravel the mysteries of N–A–S–H gel.

Recently, molecular dynamics (MD) simulation has offered an exciting opportunity to understand the N–A–S–H gel structure at nanoscale.[11] A new molecular model of N–A–S–H gel has been proposed based on the sodalite framework by Lolli.[12] The modeled N–A–S–H gel shows full Q^4 polymerization and an X-ray broad peak at 20°–30° 2θ. As geopolymer binder phase shows remarkable similarities with sodium aluminosilicate (NAS) glasses, an NAS model has been built from an initial configuration of silica glass to investigate the properties of geopolymer binders by Sadat.[13] It has been found that the structure of NAS model, including the amount of edge-sharing tetrahedra, non-bridging oxygen, and pentacoordinate Al atoms, has a huge impact on the mechanical performance. Zhang et al. have also constructed an NAS model and then applied the grand-canonical Monte Carlo method to obtain an N–A–S–H model to study the effect of water on the properties of N–A–S–H gel.[14] Besides, the geopolymerization process has been simulated through reactive MD by Zhang.[15] The simulation started from aluminate and silicate monomers and formed geopolymer gel at the end with the use of reactive Feuston−Garofalini interatomic potentials.[16]

However, the information gained from the N–A–S–H models proposed in the literature is not consistent. According to Wang's simulation,[17] N–A–S–H gel with a higher Si/Al ratio has longer Si–O and Al–O bonds, whereas Kupwade-Patil found an opposite phenomenon according to the first peak of radial distribution function.[18] Lolli assumed that all Al were tetracoordinated in the simulation.[12] Zhang also obtained simulated geopolymer gel with all Al sites in form of tetrahedrons.[15] On the contrary, pentacoordinated Al was found in N–A–S–H models in Refs. [13, 14]. As the properties of N–A–S–H gel closely rely on its composition and structure, the effect of Si/Al

ratio on the elastic modulus of N–A–S–H gel is still a matter of debate. In Wang's results, N–A–S–H gel with an Si/Al ratio of 1 has a large elastic modulus than that of 2,[17] whereas elastic modulus showed a mildly increasing trend with an increasing Si/Al ratio from 1 to 2 in Ref. [12]. Sadat recommended that an optimal Si/Al ratio at 2–3 in terms of the enhanced mechanical properties.[13] These discrepancies indicate that the atomic structures of N–A–S–H gels at different Si/Al ratios and their mechanical properties are still unclear. Further effort is required to gain a deeper understanding of atomic structures of N–A–S–H gels with different Si/Al ratios.

In this study, the formation and structure of N–A–S–H gels with different Si/Al ratios are investigated by MD simulation. Unlike most of the researches mentioned previously, the N–A–S–H gel model was obtained from the reaction of Si and Al monomers in this work. The process of polymerization was simulated and evaluated by Q^n development. A detailed structural analysis was performed on the final simulated structure, including bond length distribution, bond angle distribution, X-ray diffraction, Q^n distribution, and structure factor.

2 | METHODOLOGY

In this article, three types of molecules, including $Si(OH)_4$, $Al(OH)_3$, and $NaOH$, were employed to simulate the polymerization process by MD method. The methodology to construct N–A–S–H gel model was derived from the polymerization of silica sols first introduced by Feuston.[19] Similar approaches have been applied successfully to model the formation of the C–S–H structure by Dolado[20] and to construct geopolymer gel by Zhang.[15] Reactive force field (ReaxFF), developed by A.C.T Van Duin,[21] was adopted in this work to carry out MD simulation. Compared with traditional force fields, ReaxFF is able to accomplish chemical reactions for two reasons. One reason is that each type of atom in ReaxFF has a unique identity, which makes the atom migratable in different chemical environments during reaction process. Another key advantage of ReaxFF is the employment of bond order, which allows for the creation and dissociation of bonds during simulation.[22, 23] The detailed potential functions can be found in Refs. [24, 25]. The force field parameters herein are based on Si/Al/O/H/Na set from Refs. [24, 26], which have been successfully employed to study aluminosilicate zeolites and geopolymers.[12, 27]

2.1 | Model construction

The initial configuration was built using the PACKMOL package.[28] $Si(OH)_4$, $Al(OH)_3$, and $NaOH$ molecules were

TABLE 1 The composition and density of initial configurations (in a cubic box with a size of $25 \times 25 \times 25$ Å^3)

Si/Al	Number of Si(OH)$_4$	Number of Al(OH)$_3$	Number of NaOH	Density (g/cm^3)
1.0	92	92	92	2.10
1.5	108	72	72	2.01
1.8	117	65	65	2.02
2.5	130	52	52	1.99
3.0	138	46	46	1.99
4.0	144	36	36	1.93

placed randomly in a cubic box. The minimum size of simulation box should be larger than the size that can reveal the general features of the simulated structure, whereas the maximum size of simulation box should be determined also based on the computational efficiency. Considering these two concerns, the size of simulation box was set at $25 \times 25 \times 25$ Å^3. A similar size of simulation box was used in Refs. [14, 15]. The molecules in the box were distant from each other at least 2 Å. The initial Si/Al ratio ranges from 1.0 to 4.0 to cover a wide range, whereas Na/Al ratio was fixed at 1 to maintain charge balance. The density of the system was set at around 2 g/cm^3, which was consistent with the experimental skeletal density of geopolymers[29] and simulation parameters in Refs. [30, 31]. The amounts of different types of molecules can be determined based on the density and Si/Al ratio, as exemplified in Table 1.

MD simulations have been executed by employing the large-scale atomic/molecular massively parallel simulator (LAMMPS).[32] To eliminate the effect of the initial atomic configuration, the system was relaxed in the canonical ensemble (NVT) at 300 K for 100 ps. Then, the temperature was raised linearly up to 2000 K for the next 100 ps and subsequently kept at 2000 K for 1 ns to accelerate the reaction. Next, the system was cooled down to 300 K at a rate of 2.2 K/ps. Finally, the system was equilibrated at 300 K for 200 ps. The total duration of the process was 2.15 ns with a time step of 0.25 fs. In the end, the system consisting of the N–A–S–H cluster, water molecules, and other small species was obtained.

2.2 | Structural and mechanical characterization

Visual MD software[33] was used to visualize the snapshots. The N–A–S–H cluster was obtained from the generated system configuration using the Open Visualization Tool.[34] Several structural features of the cluster were analyzed. Bond length and bond angle were calculated based on the coordinate information. The XRD patterns were sim-

ulated by the virtual diffraction method[35] implemented in LAMMPS: The X-ray diffraction intensity was computed by the structure factor equations. Q^n distribution was calculated by counting the number of different types of Q^n to reveal the topology of the N–A–S–H gel. The partial and total structure factor functions were calculated using the Debyer package.[36] The partial structure factor, $S_{ij}(q)$, can be calculated from the Fourier transformation of the partial PDF $g_{ij}(r)$ as

$$S_{ij}(q) =$$

$$\frac{\rho_0 x_i x_j b_i(q) b_j(q) \int_0^R 4\pi r^2 \left[g_{ij}(r) - 1 \right] \frac{\sin(qr)}{qr} \frac{\sin(\pi R)}{\pi r/R} dr}{\left(\sum_i x_i b_i(q) \right)^2}$$

where q is the scattering vector, ρ_0 is the number density of the system, r is the distance, R is the cutoff of the radial distribution function between elements i and j, $g_{ij}(r)$, x_i, and x_j are the elemental fractions, and $b_i(q)$ and $b_j(q)$ are the neutron scattering lengths. The total structure factor function can be computed using the following equation:

$$S(q) = \sum_i \sum_j S_{ij}(q)$$

Note that the results in this paper are the average of the simulations based on the three different initial configurations of the system.

3 | RESULTS AND DISCUSSION

3.1 | Polymerization process

Si(OH)$_4$ and Al(OH)$_3$ monomers went through a polymerization process during simulation and eventually formed a three-dimensional (3D) cross-linked structure. The polymerization process can be revealed by the evolution of Q^n, as shown in Figure 1. Q^n represents the environment of Si or Al, including Si (Si^n) and Al sites (Al^n). The superscript n stands for the number of bridging oxygen that Si or Al is bonded. Figure 1 only shows the evolution of Q^n in the case of the Si/Al ratio of 1.0. The other Si/Al ratios can be found in the Supporting Information. It can be seen from Figure 1 that Q^0 occupied 100% at the beginning, which represented Si(OH)$_4$ and Al(OH)$_3$ monomers. All Si(OH)$_4$ and Al(OH)$_3$ monomers stayed randomly without any contact in the initial configuration. For Si sites, as simulation time went by, Q^0 decreased because it reacted and transferred to higher polymerized sites Q^n ($n = 1$–4). Meanwhile, Q^1 emerged first, followed by Q^2, Q^3, and
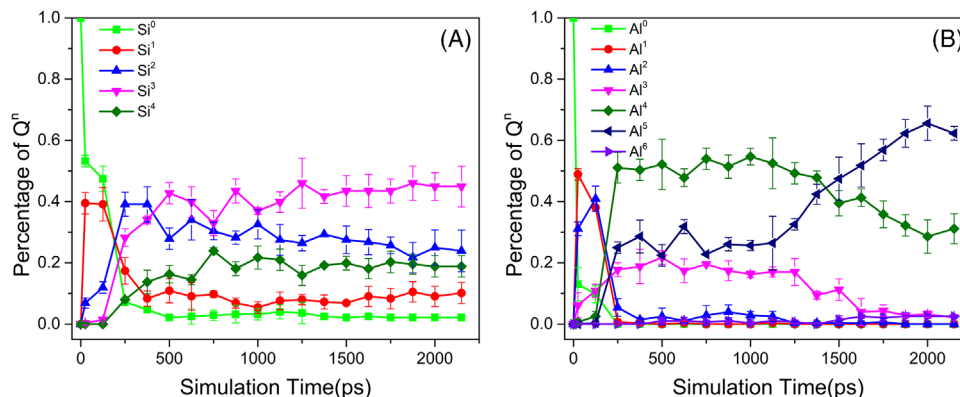
FIGURE 1 Evolution of Q^n sites for (A) Si sites and (B) Al sites (only shown the Si/Al ratio at 1.0)

Q^4 in sequence. It indicates that monomers reacted to form oligomers, and then large clusters were formed by the polymerization of oligomers. This process is in accordance with the geopolymerization process in practice.[1,37] The amount of Q^n mainly fluctuated at the beginning and reached an equilibrium state after 1250 ps. After simulation for 2150 ps, most Q^0 sites were consumed, whereas a small amount of Q^0 remained unreacted. This is because a 100% reaction degree is not possible to achieve on a realistic computational timescale. As for Al sites, their development followed similar trend to that of Si sites, which also experienced polymerization process. However, two major differences can be observed. First, all Al^0 sites were consumed completely at the end regardless of Si/Al ratios. Another interesting point is that some Al^5 sites and trace quantities of Al^6 sites were found besides Al^1, Al^2, Al^3, and Al^4. The presence of the pentacoordinate Al will be further discussed in Section 3.3.4.

The effect of the Si/Al ratio on the reaction rate can be revealed by the evolution of Q^0 sites. Figure 2 demonstrates the evolution of Si^0 sites with time at different Si/Al ratios. It is clear in Figure 2 that Si^0 declines most rapidly and dramatically at the lowest Si/Al ratio. The drop of Si^0 becomes more and more steady as the Si/Al ratio increases. In the end, the higher Si/Al ratio leads to a larger fraction of remaining Si^0. As the $Al(OH)_3$ monomers (Al^0 sites) are all consumed, based on the decreasing rate and degree of Si^0, it can be found that lower Si/Al ratio leads to faster reaction rate and a higher degree of polymerization.

Figure 3 shows the evolution of Si^0 and Al^0 for the Si/Al ratio at 1.0 and 4.0, respectively. From the comparison between the lowest Si/Al and largest Si/Al ratios, Si/Al ratio does not have a strong influence on the reaction rate of Al sites. It can be seen that the percentage of Al^0 sites plummet to 0 at the early stage regardless of the Si/Al ratios. Besides, Al was consumed earlier and faster than
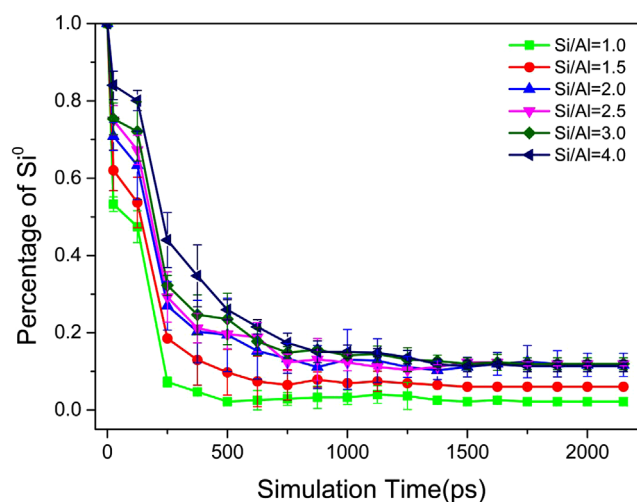

FIGURE 2 Evolution of Si^0 sites as time at different Si/Al ratios

Si according to their decreasing trend, which is in accord with the experimental finding that Al-rich gel formed at the early age and transformed into Si-rich gel later during polymerization.[38,39]

3.2 | Cluster analysis

After polymerization, all of the final configurations with different Si/Al ratios contain a 3D cross-linked network (the biggest cluster, proved to be N–A–S–H gel hereinafter), some small species, some water molecules, and some individual atoms. Among them, N–A–S–H gel, the oligomers, and water molecules are the reaction products, whereas the rest species and individual atoms are the unreacted components. The snapshot of one of the final configurations is shown in Figure 4 left, as an example to observe the aforementioned assemblage. The biggest
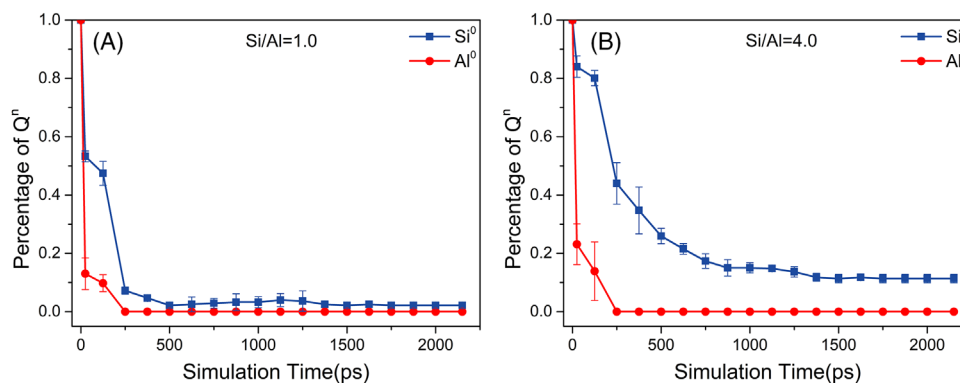
FIGURE 3 Comparison between evolution of Si^0 and Al^0 for (A) Si/Al = 1.0, (B) Si/Al = 4.0

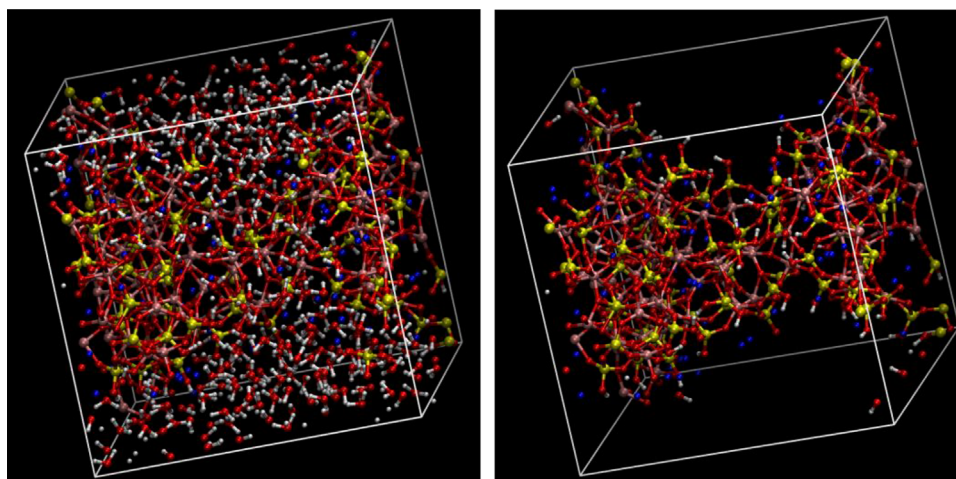**FIGURE 4** Snapshot of the whole system (left) and N–A–S–H gel model for Si/Al = 1(right); yellow refers to Si, pink refers to Al, red refers to O, white refers to H, and blue refers to Na

TABLE 2 Si/Al ratio of the initial configuration and obtained N–A–S–H model

Initial Si/Al ratio	Si/Al ratio of N–A–S–H	Formula of N–A–S–H
1.0	0.99	$Na_{77}Al_{92}Si_{91}O_{404}H_{91}$
1.5	1.38	$Na_{58}Al_{72}Si_{102}O_{402}H_{122}$
2.0	1.78	$Na_{52}Al_{60}Si_{106}O_{397}H_{138}$
2.5	1.98	$Na_{37}Al_{52}Si_{103}O_{378}H_{151}$
3.0	2.28	$Na_{31}Al_{46}Si_{105}O_{381}H_{173}$
4.0	2.75	$Na_{21}Al_{36}Si_{99}O_{346}H_{167}$

cluster was extracted from the whole system to further study the structure of N–A–S–H gel, as shown in Figure 4 right. Snapshots of configurations with the other Si/Al ratio are provided in Supporting Information. The Si/Al ratio and the chemical composition of the obtained N–A–S–H gel are shown in Table 2. The Si/Al ratio of the obtained N–A–S–H gel is slightly lower than the initial Si/Al ratio. This difference is increasingly obvious with a higher Si/Al ratio. This is because more Si remained as Si^0 site in a system with a higher Si/Al ratio, as can be seen in Figure 2. Moreover, this indicates that N–A–S–H gel with high Si/Al ratio (higher than 3) is not preferred to form. The reason behind relates to the bond energy of Si–O–Al and Si–O–Si, which will discuss hereinafter. It should be

TABLE 3 Average bond length of N–A–S–H model compared to other work

Bonds	This work	Sadat et al.[41]	Wang et al.[17]	White et al.[42]
Si–O (Å)	1.61–1.62	1.61	1.65–1.67	1.63
Al–O (Å)	1.85–1.86	1.77	1.75–1.77	1.80

noted that the Si/Al ratio in the following parts still refers to the initial Si/Al ratio in the system.

3.3 | Structural properties of simulated N–A–S–H gels

3.3.1 | Bond length

Bond length and bond angle are two basic parameters to describe the atomic structural feature of N–A–S–H gel. Both of them can be calculated based on the atomic coordinate information. The average bond lengths for Si–O and Al–O are shown in Table 3. The average Si–O bond length at around 1.62 Å is shorter than the Al–O bond length at around 1.85 Å. It is well known that longer bond length associates with smaller bond energy.[40] A reaction with smaller energy barrier is easier to happen. This can explain why Al sites react more quickly and earlier than Si sites as mentioned earlier. The average Si–O and Al–O bond lengths are compared with another simulated work from Wang,[17] Sadat,[41] and experimental results from White,[42] as also shown in Table 3. The average Si–O bond length is in good agreement with both simulated and experimental results. However, the average Al–O bond length in this work is a bit longer than that from other works. More interestingly, the average Al–O bond length of N–A–S–H gel built in this work is a bit longer than the experimental result,[42] whereas both Al–O bond lengths from the other simulation works[17,41] are shorter than the experimental result.[42] The underlying reason lies in the difference of the amount of pentacoordinate Al in the N–A–S–H structure. The Al–O bond length for pentacoordinate Al is found longer than that for tetrahedral coordinated Al. The N–A–S–H structure formed by Wang does not have pentacoordinate Al, and the N–A–S–H structure formed by Sadat only has a very small amount of pentacoordinate Al. As a result, the Al–O bond length from these two researches is shorter than the experimental value. Based on the distribution of Al sites in Section 3.3.4, there are more than 40% pentacoordinate Al in the N–A–S–H structures built in this work. This makes the average Al–O bond length a little bit longer than those from other works.

The distributions of Si–O and Al–O bond lengths for all N–A–S–H gels with different Si/Al ratios are shown in Figure 5. A small shift to the right can be both observed from the Si–O and Al–O bond length distribution curves as the Si/Al ratios increased from 1.0 to 4.0. That means a higher Si/Al ratio leads to a longer bond length. This finding is supported by Wang's research.[17]

3.3.2 | Bond angle

As [SiO_4] and [AlO_4] tetrahedrons are the basic units of an N–A–S–H gel, two types of bond angles, that is, O–T–O and T–O–T (T refers to Si or Al), were characterized. Figure 6 illustrates the distribution of O–Si–O and O–Al–O bond angles for all N–A–S–H models. The distribution of O–Si–O bond angle has a main peak at around 110° regardless of the Si/Al ratios. Compared with O–Si–O, two main differences can be noticed from the distribution of the O–Al–O bond angle: (i) O–Al–O bond angle has a much broader range than that of O–Si–O; (ii) the distribution of O–Al–O bond angle exhibits two humps at around 95° and 150°, respectively. These two features indicate that Al environments are richer than that of Si. That indicates the existence of Al provides N–A–S–H gel with a more flexible skeleton. According to the previous Q^n information and snapshot, all Si exist as SiO_4 tetrahedrons in the obtained N–A–S–H models, whereas the Al environments include AlO_4 tetrahedrons and AlO_5 nontetrahedrons. In a regular tetrahedron, the O–T–O bond angles are 120°. That is why the O–Si–O bond angles in SiO_4 tetrahedrons mainly correspond to the range from 95° to 125°. However, the O–Al–O bond angles in an AlO_5 non-tetrahedral structure can range from an acute angle to a very large obtuse angle. Therefore, there is an amount of O–Al–O bond angle located at around 80° and 150°, respectively.

There are three types of T–O–T bond angles in the obtained N–A–S–H structures, i.e. Al–O–Al, Si–O–Al, and Si–O–Si. The fraction of these T–O–T bond angles is shown in Figure 7. As can be seen in Figure 7, Si–O–Al accounts for the majority (around 70%) of T–O–T bond angles. Si–O–Si only represents a small proportion even at high Si/Al ratios. This indicates that an [SiO_4] tetrahedron tends to link with an [AlO_4] tetrahedron instead of an [SiO_4] tetrahedron. It is interesting to note that small percentages of Al–O–Al bond angle can be found in all the obtained N–A–S–H models. Although Loewenstein's rule of nearest-neighbor Al avoidance is widely obeyed in many researches, Al–O–Al is not strictly forbidden and has been found in some cases.[15,43–46] The presence of Al–O–Al is
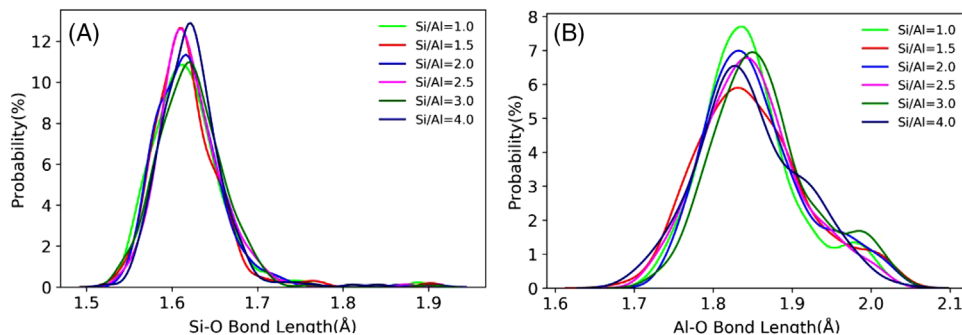
FIGURE 5 Bond length distribution of (A) Si–O and (B) Al–O for all N–A–S–H gel models
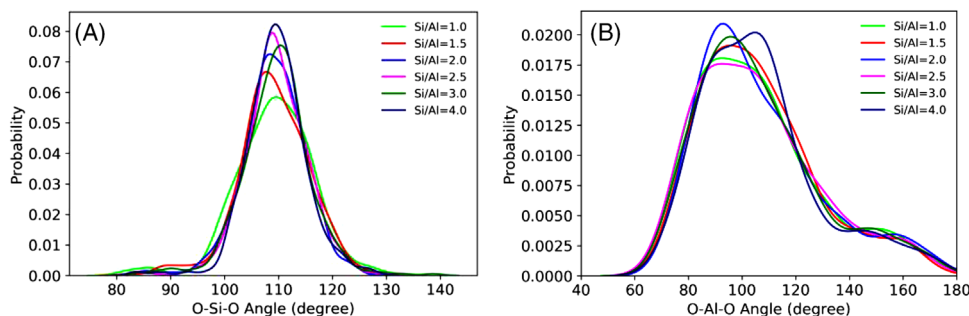

FIGURE 6 Bond angle distribution of: (A) O–Si–O and (B) O–Al–O for all N–A–S–H gel models
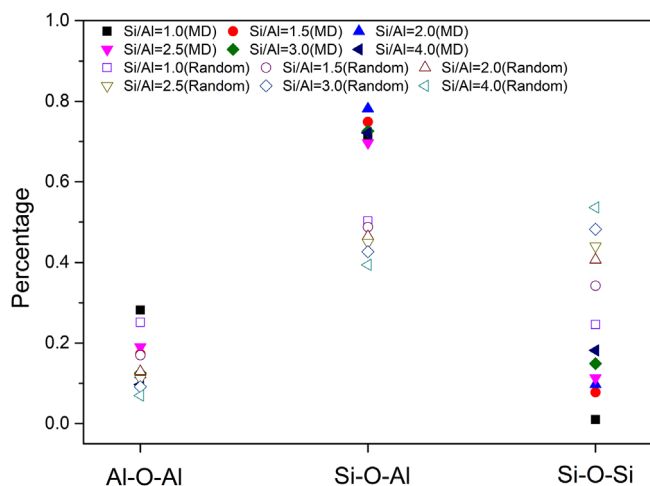

FIGURE 7 Fraction of different types of T–O–T bond angle for all N–A–S–H gel models

supported by both the experimental results[45] and simulation results.[15,46] To further evaluate the ordering of Si and Al cations in N–A–S–H structures, the probabilities forming these three types of T–O–T bond angles were calculated through the following equations by assuming a random distribution of Si and Al around bridging oxygens[48,49]:

$$P_{Si-O-Si} = \frac{N_{Si}(N_{Si}-1)}{(N_{Si}+N_{Al})(N_{Si}+N_{Al}-1)}$$

$$P_{Al-O-Al} = \frac{N_{Al}(N_{Al}-1)}{(N_{Si}+N_{Al})(N_{Si}+N_{Al}-1)}$$

$$P_{Si-O-Al} = \frac{2N_{Si}N_{Al}}{(N_{Si}+N_{Al})(N_{Si}+N_{Al}-1)}$$

where N_{Si} and N_{Al} are the numbers of Si and Al atoms, respectively. It can be seen from Figure 7 that the proportion of Al–O–Al from MD simulation is similar to that from random distribution. However, the amount of Si–O–Al from MD simulation is higher than that from random distribution, whereas a converse situation is found in the case of Si–O–Si. These differences confirm that an Si site has higher tendency to connect to an Al site compared to an Si site. Similar results were found in Ref. [49].

Figure 8 shows the distribution of T–O–T bond angles. The Al–O–Al bond angle has a main peak at around 150°, whereas the Si–O–Si bond angle is mainly located at 140°, both of them are in a good agreement with Ref. [46]. A very broad peak can be seen in the range of 80°–180° for the Si–O–Al bond angle, which indicates the existence of different types of Si–O–Al sites. According to Walkley,[10] the mean Si–O–Al bond angle is at around 143.4° in Na⁺-balanced Si⁴–O–Al⁴ sites and at around 124.4° in
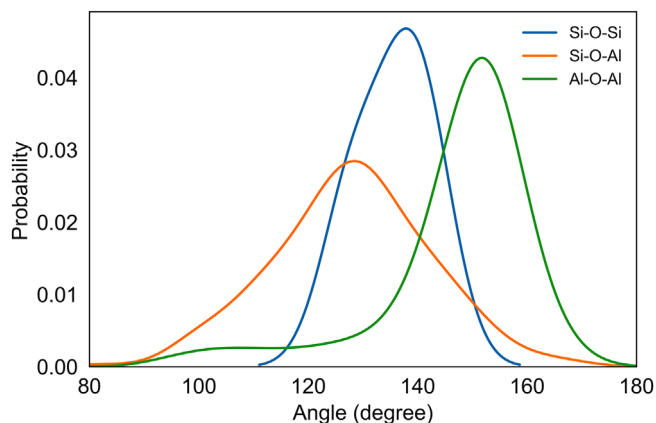
FIGURE 8 Bond angle distribution of Al–O–Al, Si–O–Al, and Si–O–Si for N–A–S–H gel with Si/Al ratio of 1

Na^+/Al^{EF}-balanced Si^4-O-Al^4 sites. This result confirms that Si–O–Al has different environments corresponding to different bond angles.

3.3.3 | X-ray diffraction

X-ray diffraction patterns can further verify the amorphous nature of the obtained N–A–S–H. A broad peak from 20° to 40°, typical hump for N–A–S–H gel,[3,50] can be observed for all XRD patterns with different Si/Al ratios in Figure 9. Besides, a visible shift toward the small angle can be seen as the Si/Al ratio increases. Identical results were obtained in Lee's work, where the typical hump is located at 28.54°, 26.85°, and 26.27° for the geopolymer paste with Si/Al ratios of 1.5, 3.5, and 4.0, respectively.[51] Lee believed this difference was a result of different degree of polymerization. More specifically, the shift from 23.14° (the XRD peak for fly ash) before polymerization to 28.54° (geopolymer paste with Si/Al ratio of 1.5) is believed to associate with a higher degree of polymerization than the one from 23.14° to 26.27° (geopolymer paste with Si/Al ratio of 4.0). Obviously, such opinion does not consider the structures of N–A–S–H gels with different Si/Al ratios. Hence, it cannot explain why lower Si/Al ratio of N–A–S–H gel leads to a shift to a larger angle in an XRD pattern for N–A–S–H gel. In this work, the probable reason for lower Si/Al ratio located at higher 2θ angle is that N–A–S–H gel structure with lower Si/Al ratio is more compact than that with higher Si/Al ratio. According to Bragg's law, a higher angle corresponds to a smaller interplanar spacing. From the aforementioned analysis of bond length, the N–A–S–H gel structure with lower Si/Al ratio has shorter Si–O and Al–O bond lengths, indicating a more compact structure with smaller interplanar spacing. That is why the XRD hump for the N–A–S–H gel structure with lower Si/Al ratio is

centered on higher 2θ angle compared to that with higher Si/Al ratio.

3.3.4 | Q^n distribution

Q^n distribution is the most important structural index to explain how Si and Al are linked in the framework. Generally, Q^1 belongs to the end sites; Q^2 represents the middle groups in chains or cycles; Q^3 refers to branched structure; and Q^4 indicates a fully cross-linked structure, like rings or cages.[52,53] The Si sites (Si^n) distribution for all N–A–S–H structures with different Si/Al ratios is illustrated in Figure 10. Four types of Si^n units, Si^1, Si^2, Si^3, and Si^4, were found in all N–A–S–H structures, indicating a complex network. Si^0 is not shown because already excluded. The total proportions of Si^3 and Si^4 range from 38% to 65%. This is lower compared with the experimental data from Refs. [45, 54]. According to these studies, Si mainly exists in the form of Q^4 in N–A–S–H gel framework. A small amount of Q^1 is doubtless present at the surface of the gel. The lower percentage of Si^3 and Si^4 in the simulated structure is probably due to the size of the simulated system. A system containing around 1000 atoms is not a large system. As a result, the final obtained structure is not a big enough cluster and, thus, has a large surface containing more Si^1 and Si^2. The connectivity of the obtained structure relies on the amount of high polymerized Si sites, that is, Si^3 and Si^4. Thus, the ratio (Si^3 and Si^4)/(Si^1 and Si^2) is a meaningful index to reveal the effect of Si/Al ratio on the connectivity of the structure. A similar parameter called the Q factor was used to investigate the structure of C–S–H gel in Ref. [20, 55]. As can be seen from Figure 11, there is an overall downward trend in the ratio (Si^3 and Si^4)/(Si^1 and Si^2) as Si/Al ratios increase from 1.0 to 4.0. That means the structures at lower Si/Al ratios (e.g., 1.0 or 1.5) are more cross-linked compared with those at higher Si/Al ratios (e.g., 3.0 and 4.0). This result has confirmed the fact that lower Si/Al ratios tend to form a 3D network (more Si^3 and Si^4), whereas higher Si/Al ratios prefer a 2D cross-linked structure (more Si^1 and Si^2).[56,57]

The environment for Si^4 is complex, containing five possible silicon species $Si^4(mAl)$, where m (m = 0,1,2,3,4) refers to the number of Al connected to the Si^4 tetrahedron. Thus, the analysis of the distribution of $Si^4(mAl)$ can further understand the connectivity between Si and Al. The fraction of five $Si^4(mAl)$ sites is shown in Figure 12. $Si^4(4Al)$ is the major Si^4 site for the structure with lower Si/Al ratios. When the Si/Al ratio comes to 4.0, $Si^4(3Al)$ makes up the largest proportion of $Si^4(mAl)$ sites instead of $Si^4(4Al)$. Generally, $Si^4(3Al)$ and $Si^4(4Al)$ are the two main Si^4 sites for all the structures in this study. The distribution of $Si^4(mAl)$ in this study is similar to the results from
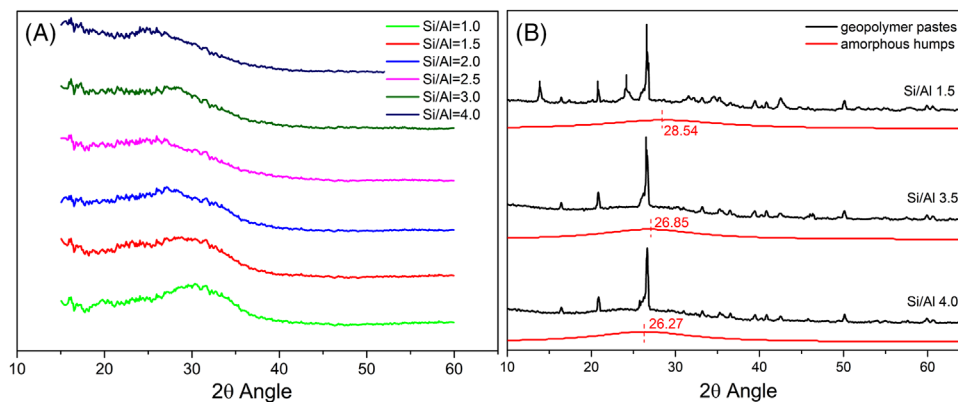
FIGURE 9 X-ray diffraction (XRD) patterns for: (A) all simulated N–A–S–H structures with different Si/Al ratios and (B) geopolymer paste at the age of 28 days adapted from Lee [51]
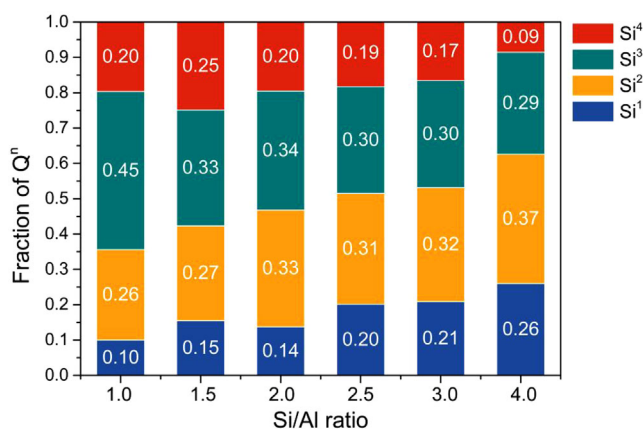

FIGURE 10 Distribution of Si^n sites within all N–A–S–H gel models with different Si/Al ratios

FIGURE 11 $(Si^3$ and $Si^4)/(Si^1$ and $Si^2)$ as a function of Si/Al ratio

Lyu[58] and Duxson,[45] as also shown in Figure 12. These results indicate that an Si^4 tetrahedron tends to connect with more than 2 Al tetrahedrons. ^{29}Si MAS NMR experimental results also show that polyhedral connection is mainly Al–O–Si–O–Al in zeolites with Si/Al of 1–3.[60,61] The mechanism behind this lies in that Si–O–Al is preferred over Si–O–Si to be formed from the thermodynamic and kinetic point of view.[61,62]

The reason for the different tendency of cross-link with different Si/Al ratios is now clear. The results of bond angle and $Si^4(m\mathrm{Al})$ reveal that Si site would link with Al site in preference. That means an Si site can link with 3–4 Al sites in an Al-rich system but unlikely link with 3–4 Si sites in an Si-rich system. As a result, more Q^3 and Q^4 are more likely to form in an Al-rich system, whereas more Q^1 and Q^2 tend to form in an Si-rich system. The distribution of Q^n would determine the degree of polymerization of a structure. In this study, N–A–S–H gel structure became more depolymerized as Si/Al was increased, which is in accordance with the findings in Ref. [49].
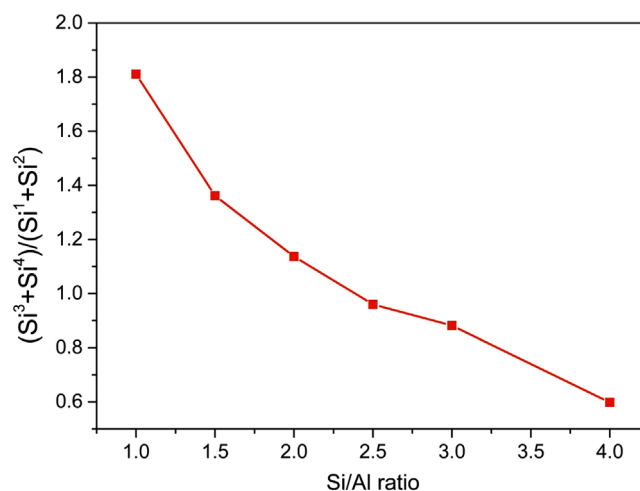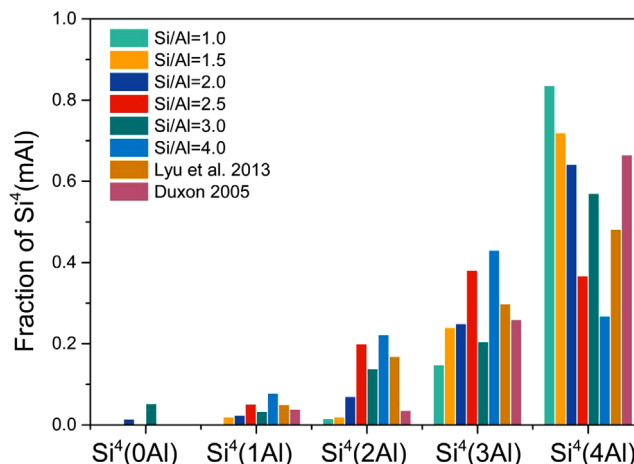

FIGURE 12 Distribution of $Si^4(m\mathrm{Al})$ within all N–A–S–H gel models with different Si/Al ratios
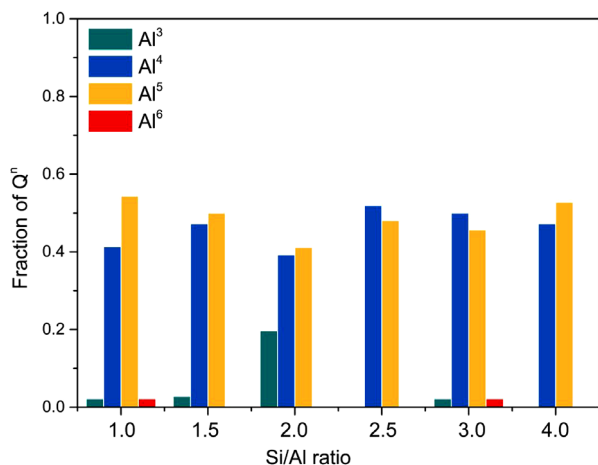
FIGURE 13 Distribution of Al^n sites within all N–A–S–H gel models with different Si/Al ratios

FIGURE 14 Neutron structure factor predicted for all N–A–S–H gel models with different Si/Al ratios

The distribution of Al is shown in Figure 13. Al^4 and Al^5 are two main Al sites for all the simulated structures with different Si/Al ratios. It is generally believed that Al always stays tetrahedrally coordinated and Al^4 is the main existing form based on NMR results.[38,7] As previously mentioned, pentacoordinate Al and six coordinated Al were once believed to only come from the unreacted raw materials in geopolymer pastes[63,7] until Walkley proposed an N–A–S–H model containing six coordinated Al for the first time.[10] These six coordinated Al atoms are considered a charge-balance role like Na^+ ions to compensate Al tetrahedrons. Actually, pentacoordinate Al and six coordinated Al have been found as the charge-balance roles in aluminosilicate glass system in many early reports.[64–66] It usually happens when there are excess Al and insufficient cations. In this study, traces of Al^6 sites were found during simulation. The non-tetrahedral Al mainly exists as Al^5. The presence of Al^5 is also detected in some N–A–S–H structures built by MD.[14,30,67] Around 40%–50% of pentacoordinate Al was formed in the final obtained structures in this study, which is consistent with the result in Zhang's work (45.2%).[14]

The reason that Al^5, Al^6, and Al–O–Al can form is discussed as follows: Monomers, representing the dissolved components from raw materials, were employed in the starting configuration. A reaction path mimicking polymerization was followed by using ReaxFF during MD simulation. No extra condition was imposed to interfere with the simulation process. The movements of the atoms only depend on the atomic interaction. This whole simulation process was close to reality. In contrast, some assumptions were made before simulation. For example, Loewenstein's principle and full Q^4 were obeyed in Ref [12]. As a result, it would not have Al–O–Al and non-tetrahedral Al in the obtained structure.
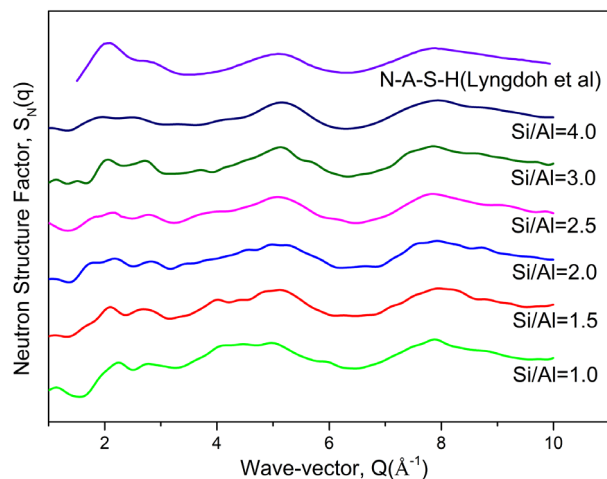
3.3.5 | Structure factor

The structure factor was calculated to reveal an N–A–S–H gel structure of medium-range order, as shown in Figure 14. For all N–A–S–H gels structures, four peaks can be observed at Q values of around 2–3, 5, and 8 $Å^{-1}$. The locations of these peaks match well with that of the simulated N–A–S–H gel,[68] as shown in Figure 14. Geopolymer pastes also showed similar patterns.[69] A minor difference is that the intensity of the hump at around 2 $Å^{-1}$ was not as strong as those in Refs. [68, 69]. This peak was supposed to be introduced by water according to neutron total scattering data.[42, 69] As N–A–S–H gels in this work do not contain interlayer water, it is reasonable that the peak at 2 $Å^{-1}$ was lower than that in Ref [68].

4 | CONCLUSIONS

This work provides a new way to build the N–A–S–H gel model by MD simulation. The N–A–S–H atomic model was built successfully by reactive MD simulation from a polymerization point of view. The simulated polymerization process was evaluated by the development of Q^n sites. The obtained N–A–S–H gel was a 3D network consistent with existing experimental or simulation results in terms of bond length, bond angle, XRD, Q^n distribution, and structure factor. The main findings are summarized as follows:

1. During the simulation, the system went through a polymerization process similar to what happened in real geopolymerization. With ReaxFF, the system containing Si monomers, Al monomers, and NaOH eventually developed into a cross-link network (N–A–S–H gel),

together with oligomers, water molecules, and other species.

2. The highly broad range of O–Al–O and Si–O–Al bond angles reveals a complicated Al environment. The presence of Al–O–Al proves that Loewenstein's rule is not always correct in geopolymer. Pentacoordinate Al was found in N–A–S–H model, demonstrating that Al does not 100% exist as tetrahedral forms in reaction products. This finding is against the previous view that pentacoordinate Al in geopolymer only comes from raw materials. The comparison of proportions of different T–O–T bond angles between random distribution and simulation confirms that Si–O–Al is preferred to form among three types of T–O–T bond angles.

3. The soundness of N–A–S–H gel was assessed from not only short-range order but also medium-range order. All structure factor peaks match closely with experimental and other simulation results in the literature, meaning that the N–A–S–H gel structures obtained in this work are convincing.

4. Si/Al ratio can affect the structure of N–A–S–H gel. As Si/Al ratio increases, both Si–O and Al–O bond lengths become longer. The typical hump in XRD patterns shifts to smaller angle (larger d spacing) with the increase of Si/Al ratio. More highly polymerized Si^n sites (i.e., Si^3 and Si^4) were formed in the structure with lower Si/Al ratio. All of these results indicate that N–A–S–H gel with lower Si/Al ratio is more compacted and stable.

The simulation results of this study provide new insight regarding the Al environment in geopolymer. The knowledge of N–A–S–H structure with different Si/Al ratios can be a key to further investigate the behaviors of geopolymer and to guide a mixed design of satisfactory geopolymers.

CONFLICT OF INTEREST

The authors declare that there is no conflict of interest that could be perceived as prejudicing the impartiality of the research reported.

ORCID

Yun Chen https://orcid.org/0000-0003-1980-2460
Zhenming Li https://orcid.org/0000-0002-6752-6264

REFERENCES

1. Duxson P, Fernández-Jiménez A, Provis JL, Lukey GC, Palomo A, Van Deventer JSJ. Geopolymer technology: the current state of the art. J Mater Sci. 2007;42:2917–33. https://doi.org/10.1007/s10853-006-0637-z

2. Provis JL, Palomo A. Advances in understanding alkali-activated materials. Cem Concr Res. 2015;78:110–25. https://doi.org/10.1016/J.CEMCONRES.2015.04.013

3. Criado M, Fernández-Jiménez A, de la Torre AG, Aranda MAG, Palomo A. An XRD study of the effect of the SiO_2/Na_2O ratio on the alkali activation of fly ash. Cem Concr Res. 2007;37:671–9. https://doi.org/10.1016/j.cemconres.2007.01.013

4. Provis JL, Lukey GC, Van Deventer JSJ. Do geopolymers actually contain nanocrystalline zeolites? a reexamination of existing results. Chem Mater. 2005;17:3075–85. https://doi.org/10.1021/cm050230i

5. Fernández-Jiménez A, Palomo A. Mid-infrared spectroscopic studies of alkali-activated fly ash structure. Microporous Mesoporous Mater. 2005;86:207–14. https://doi.org/10.1016/j.micromeso.2005.05.057

6. Rees CA, Provis JL, Lukey GC, Van Deventer JSJ. In situ ATR-FTIR study of the early stages of fly ash geopolymer gel formation. Langmuir. 2007;23:9076–82. https://doi.org/10.1021/la701185g

7. Palomo A, Alonso S, Fernandez-Jimeťnez A. Alkaline activation of fly ashes: NMR study of the reaction products. J Am Ceram Soc. 2004;87:1141–5. https://ceramics.onlinelibrary.wiley.com/doi/pdf/10.1111/j.1551-2916.2004.01141.x (accessed 10 May 2019)

8. Rowles MR, Hanna JV, Pike KJ, Smith ME., O'Connor BH. ^{29}Si, ^{27}Al, ^1H and ^{23}Na MAS NMR study of the bonding character in aluminosilicate inorganic polymers. Appl Magn Reson. 2007;32:663–89. https://doi.org/10.1007/s00723-007-0043-y

9. Walkley B, San Nicolas R, Sani MA, Gehman JD, Van Deventer JSJ, Provis JL. Phase evolution of $Na_2O-Al_2O_3-SiO_2-H_2O$ gels in synthetic aluminosilicate binders. Dalton Trans. 2016;45:5521–35. https://doi.org/10.1039/c5dt04878h

10. Walkley B, Rees GJ, San Nicolas R, Van Deventer JSJ, Hanna JV, Provis JL. New structural model of hydrous sodium aluminosilicate gels and the role of charge-balancing extra-framework Al. J Phys Chem C. 2018;122:5673–85. https://doi.org/10.1021/acs.jpcc.8b00259

11. Xu LY, Alrefaei Y, Wang YS, Dai JG. Recent advances in molecular dynamics simulation of the N-A-S-H geopolymer system: modeling, structural analysis, and dynamics. Constr Build Mater. 2021;276:122196. https://doi.org/10.1016/j.conbuildmat.2020.122196

12. Lolli F, Manzano H, Provis JL, Bignozzi MC, Masoero E. Atomistic simulations of geopolymer models: the impact of disorder on structure and mechanics. ACS Appl Mater Interfaces. 2018;10:22809–20. https://doi.org/10.1021/acsami.8b03873

13. Sadat MR, Bringuier S, Muralidharan K, Runge K, Asaduzzaman A, Zhang L. An atomistic characterization of the interplay between composition, structure and mechanical properties of amorphous geopolymer binders. J Non-Cryst Solids. 2016;434:53–61. https://doi.org/10.1016/J.JNONCRYSOL.2015.11.022

14. Zhang Y, Zhang J, Jiang J, Hou D, Zhang J. The effect of water molecules on the structure, dynamics, and mechanical

properties of sodium aluminosilicate hydrate (NASH) gel: a molecular dynamics study. Constr Build Mater. 2018;193:491–500. https://doi.org/10.1016/J.CONBUILDMAT.2018.10.221

15. Zhang M, Deskins NA, Zhang G, Cygan RT, Tao M. Modeling the polymerization process for geopolymer synthesis through reactive molecular dynamics simulations. J Phys Chem C. 2018;122:6760–73. https://doi.org/10.1021/acs.jpcc.8b00697

16. Feuston BP, Garofalini SH. Oligomerization in silica sols. J Phys Chem. 1990;94:5351–6. https://doi.org/10.1021/j100376a035

17. Wang R, Wang J, Dong T, Ouyang G. Structural and mechanical properties of geopolymers made of aluminosilicate powder with different SiO_2/Al_2O_3 ratio: molecular dynamics simulation and microstructural experimental study. Constr Build Mater. 2020;240:117935. https://doi.org/10.1016/j.conbuildmat.2019.117935

18. Kupwade-Patil K, Soto F, Kunjumon A, Allouche EN, Mainardi DS. Multi-scale modeling and experimental investigations of geopolymeric gels at elevated temperatures. Comput Struct. 2013;122:164–77. https://doi.org/10.1016/j.compstruc.2013.01.005

19. Feuston BP, Garofalini SH. Onset of polymerization in silica sols. Chem Phys Lett. 1990;170:264–70. https://doi.org/10.1016/0009-2614(90)87126-C

20. Dolado JS, Griebel M, Hamaekers J. A molecular dynamic study of cementitious calcium silicate hydrate (C-S-H) gels. J Am Ceram Soc. 2007;90:3938–42. https://doi.org/10.1111/j.1551-2916.2007.01984.x

21. Van Duin ACT, Strachan A, Stewman S, Zhang Q, Xu X, Goddard WA. ReaxFFSiO reactive force field for silicon and silicon oxide systems. J Phys Chem A. 2003;107:3803–11. https://doi.org/10.1021/jp0276303

22. Van Duin ACT, Dasgupta S, Lorant F, Goddard WA. ReaxFF: a reactive force field for hydrocarbons. J Phys Chem A. 2001;105:9396–409. https://doi.org/10.1021/jp004368u

23. Mishra RK, Mohamed AK, Geissbühler D, Manzano H, Jamil T, Shahsavari R, et al. cemff: a force field database for cementitious materials including validations, applications and opportunities. Cem Concr Res. 2017;102:68–89. https://doi.org/10.1016/J.CEMCONRES.2017.09.003

24. Joshi KL, Van Duin ACT. Molecular dynamics study on the influence of additives on the high-temperature structural and acidic properties of ZSM-5 zeolite. Energy Fuels. 2013;27:4481–4488. https://doi.org/10.1021/ef3020124

25. Fogarty JC, Aktulga M, Grama AY, Van Duin ACT, Pandit SA. A reactive molecular dynamics simulation of the silica-water interface. J Phys Chem. 2010;132:174704. https://doi.org/10.1063/1.3407433

26. Joshi KL, Psofogiannakis G, Van Duin ACT, Raman S. Reactive molecular simulations of protonation of water clusters and depletion of acidity in H-ZSM-5 zeolite. Phys Chem Chem Phys. 2014;16:18433–41. https://doi.org/10.1039/c4cp02612h

27. Psofogiannakis GM, McCleerey JF, Jaramillo E, Van Duin ACT. ReaxFF reactive molecular dynamics simulation of the hydration of Cu-SSZ-13 zeolite and the formation of Cu dimers. J Phys Chem C. 2015;119:6678–86. https://doi.org/10.1021/acs.jpcc.5b00699

28. Allouche A. Software news and updates gabedit — a graphical user interface for computational chemistry softwares. J Comput Chem. 2012;32:174–82. https://doi.org/10.1002/jcc

29. Šmilauer V, Hlaváček P, Škvára F, Šulc R, Kopecký L, Němeček J. Micromechanical multiscale model for alkali activation of fly ash and metakaolin. J Mater Sci. 2011;46:6545–55. https://doi.org/10.1007/s10853-011-5601-x

30. Sadat MR, Bringuier S, Asaduzzaman A, Muralidharan K, Zhang L. A molecular dynamics study of the role of molecular water on the structure and mechanics of amorphous geopolymer binders. J Chem Phys. 2016;145:134706. https://doi.org/10.1063/1.4964301

31. Chitsaz S, Tarighat A. Molecular dynamics simulation of N-A-S-H geopolymer macro molecule model for prediction of its modulus of elasticity. Constr Build Mater. 2020;243:118176. https://doi.org/10.1016/j.conbuildmat.2020.118176

32. Plimpton S. Fast parallel algorithms for short-range molecular dynamics. J Comput Phys. 1995;117:1–19. https://doi.org/10.1006/jcph.1995.1039

33. Humphrey W, Dalke A, Schulten K. VMD: visual molecular dynamics. J Mol Graphics. 1996;14:33–8.

34. Stukowski A. Visualization and analysis of atomistic simulation data with OVITO–the Open visualization tool. Modell Simul Mater Sci Eng. 2009;18:15012.

35. Coleman SP, Spearot DE, Capolungo L. Virtual diffraction analysis of Ni [0 1 0] symmetric tilt grain boundaries. Modell Simul Mater Sci Eng. 2013;21:1–16. https://doi.org/10.1088/0965-0393/21/5/055020

36. https://github.com/wojdyr/debyer, (n.d.)

37. Provis JL, van Deventer JSJ. Geopolymerisation kinetics. 2. Reaction kinetic modelling. Chem Eng Sci. 2007;62:2318–29. https://doi.org/10.1016/j.ces.2007.01.028

38. Fernández-Jiménez A, Palomo A, Sobrados I, Sanz J. The role played by the reactive alumina content in the alkaline activation of fly ashes. Microporous Mesoporous Mater. 2006;91:111–9. https://doi.org/10.1016/j.micromeso.2005.11.015

39. Rees CA, Provis JL, Lukey GC, Van Deventer JSJ. Attenuated total reflectance Fourier transform infrared analysis of fly ash geopolymer gel aging. Langmuir. 2007;23:8170–9. https://doi.org/10.1021/la700713g

40. Gordy W. Dependence of bond order and of bond energy upon bond length. J Chem Phys. 1947;15:305–10. https://doi.org/10.1063/1.1746501

41. Sadat MR, Muralidharan K, Zhang L. Reactive molecular dynamics simulation of the mechanical behavior of sodium aluminosilicate geopolymer and calcium silicate hydrate composites. Comput Mater Sci. 2018;150:500–9. https://doi.org/10.1016/j.commatsci.2018.04.041

42. White CE, Provis JL, Proffen T, Van Deventerz JSJ. The effects of temperature on the local structure of metakaolin-based geopolymer binder: a neutron pair distribution function investigation. J Am Ceram Soc. 2010;93:3486–92. https://doi.org/10.1111/j.1551-2916.2010.03906.x

43. Lee SK, Stebbins JF. Al-O-Al and Si-O-Si sites in framework aluminosilicate glasses with Si/Al = 1: quantification of framework disorder. J Non-Cryst Solids. 2000;270:260–4.

44. Stebbins JF, Lee SK, Oglesby JV. Al-O-Al oxygen sites in crystalline aluminates and aluminosilicate glasses: high-resolution oxygen-17 NMR results. Am Mineral. 1999;84:983–6. https://doi.org/10.2138/am-1999-5-635

45. Duxson P, Provis JL, Lukey GC, Separovic F, Van Deventer JSJ. ^{29}Si NMR study of structural ordering in aluminosilicate geopolymer gels. Langmuir. 2005;21:3028–36. https://doi.org/10.1021/la047336x

46. Dongol R, Wang L, Cormack AN, Sundaram SK. Molecular dynamics simulation of sodium aluminosilicate glass structures and glass surface-water reactions using the reactive force field (ReaxFF). Appl Surf Sci. 2018;439:1103–10. https://doi.org/10.1016/j.apsusc.2017.12.180

47. Pedone A, Gambuzzi E, Menziani MC. Unambiguous description of the oxygen environment in multicomponent aluminosilicate glasses from ^{17}O solid state NMR computational spectroscopy. J Phys Chem C. 2012;116:14599–609. https://doi.org/10.1201/b12066-172

48. Ren M, Deng L, Du J. Bulk, surface structures and properties of sodium borosilicate and boroaluminosilicate nuclear waste glasses from molecular dynamics simulations. J Non-Cryst Solids. 2017;476:87–94. https://doi.org/10.1016/j.jnoncrysol.2017.09.030

49. Lu X, Reiser JT, Parruzot B, Deng L, Gussev IM, Neuefeind JC, et al. Effects of Al:Si and (Al + Na):Si ratios on the properties of the international simple glass, Part II: Structure. J Am Ceram Soc. 2021;104:183–207. https://doi.org/10.1111/jace.17447

50. Gomez-Zamorano L, Balonis M, Erdemli B, Neithalath N, Sant G. C–(N)–S–H and N–A–S–H gels: compositions and solubility data at 25°C and 50°C. J Am Ceram Soc. 2017;100:2700–11. https://doi.org/10.1111/jace.14715

51. Lee B, Kim G, Kim R, Cho B, Lee S, Chon CM. Strength development properties of geopolymer paste and mortar with respect to amorphous Si/Al ratio of fly ash. Constr Build Mater. 2017;151:512–9. https://doi.org/10.1016/j.conbuildmat.2017.06.078

52. Brunet F, Cabane B, Dubois M, Perly B. Sol-gel polymerization studied through ^{29}Si NMR with polarization transfer. J Phys Chem. 1991;95:945–51. https://doi.org/10.1021/j100155a082

53. Singh PS, Bastow T, Trigg M. Structural studies of geopolymers by ^{29}Si and ^{27}Al MAS-NMR. J Mater Sci. 2005;40:3951–61. https://doi.org/10.1007/s10853-005-1915-x

54. Li Z, Zhang S, Zuo Y, Chen W, Ye G. Chemical deformation of metakaolin based geopolymer. Cem Concr Res. 2019;120:108–18. https://doi.org/10.1016/J.CEMCONRES.2019.03.017

55. Thomas JJ, Jennings HM. Free-energy-based model of chemical equilibria in the CaO-SiO$_2$-H$_2$O system. J Am Ceram Soc. 1998;81:606–12. https://doi.org/10.1111/j.1151-2916.1998.tb02380.x

56. Davidovits J. Geopolymers: inorganic polymeric new materials. J Therm Anal. 1991;37:1633–56. https://doi.org/10.1533/9781845696382

57. Davidovits J. 30 years of successes and failures in geopolymer applications. Market trends and potential breakthroughs. In: Geopolymer 2002 Conf. 2002. p. 1–16 https://doi.org/10.1017/CBO9781107415324.004

58. Lyu S, Wang T, Cheng T, Ueng T. Main factors affecting mechanical characteristics of geopolymer revealed by experimental design and associated statistical analysis. Constr Build Mater. 2013;43:589–97. https://doi.org/10.1016/j.conbuildmat.2013.02.033

59. Melchior MT, Vaughan DEW, Jacobson AJ. Characterization of the silicon-aluminum distribution in synthetic faujasites by high-resolution solid-state ^{29}Si NMR. J Am Chem Soc. 1982;104:4859–64.

60. Lippmaa E, Mägi M, Samoson A, Tarmak M, Engelhardt G. Investigation of the structure of zeolites by solid-state high-resolution ^{29}Si NMR spectroscopy. J Am Chem Soc. 1981;103:4992–6. https://doi.org/10.1021/ja00407a002

61. Provis JL, Duxson P, Lukey GC, Van Deventer JSJ. Statistical thermodynamic model for Si/Al ordering in amorphous aluminosilicates. Chem Mater. 2005;17:2976–86. https://doi.org/10.1021/cm050219i

62. Fernández-Jiménez A, de la Torre AG, Palomo A, López-Olmo G, Alonso MM, Aranda MAG. Quantitative determination of phases in the alkaline activation of fly ash. Part II: Degree of reaction. Fuel. 2006;85:1960–9. https://doi.org/10.1016/j.fuel.2006.04.006

63. Ruiz-Santaquiteria C, Skibsted J, Fernández-Jiménez A, Palomo A. Alkaline solution/binder ratio as a determining factor in the alkaline activation of aluminosilicates. Cem Concr Res. 2012;42:1242–51. https://doi.org/10.1016/j.cemconres.2012.05.019

64. Mundus C, Müller-Warmuth W. ^{27}Al magic-angle spinning nuclear magnetic resonance satellite transition spectroscopy of glasses in the system K$_2$O-Al$_2$O$_3$-SiO$_2$. Solid State Nucl Magn Reson. 1995;5:79–88.

65. Stebbins JF, Kroeker S, Lee SK, Kiczenski TJ. Quantification of five- and six-coordinated aluminum ions in aluminosilicate and fluoride-containing glasses by high-field, high-resolution ^{27}Al NMR. J Non-Cryst Solids. 2000;275:4–9.

66. Bechgaard TK, Goel A, Youngman RE, Mauro JC, Rzoska SJ, Bockowski M, et al. Structure and mechanical properties of compressed sodium aluminosilicate glasses: role of non-bridging oxygens. J Non-Cryst Solids. 2016;441:49–57. https://doi.org/10.1016/j.jnoncrysol.2016.03.011

67. Wan H, Yuan L, Zhang Y. Insight into the leaching of sodium alumino-silicate hydrate (N-A-S-H) gel: a molecular dynamics study. Front Mater. 2020;7:1–11. https://doi.org/10.3389/fmats.2020.00056

68. Lyngdoh GA, Kumar R, Krishnan NMA, Das S. Realistic atomic structure of fly ash-based geopolymer gels: insights from molecular dynamics simulations. J Chem Phys. 2019;151:064307. https://doi.org/10.1063/1.5121519

69. White CE, Provis JL, Llobet A, Proffen T, Van Deventer JSJ. Evolution of local structure in geopolymer gels: an in situ neutron pair distribution function analysis. J Am Ceram Soc. 2011;94:3532–9. https://doi.org/10.1111/j.1551-2916.2011.04515.x

SUPPORTING INFORMATION

Additional supporting information can be found online in the Supporting Information section at the end of this article.